Genome remodelling in a basal-like breast cancer metastasis and xenograft

Li Ding[1,2]*, Matthew J. Ellis[3,4]*, Shunqiang Li[3], David E. Larson[1], Ken Chen[1], John W. Wallis[1,2], Christopher C. Harris[1], Michael D. McLellan[1], Robert S. Fulton[1,2], Lucinda L. Fulton[1,2], Rachel M. Abbott[1], Jeremy Hoog[3], David J. Dooling[1,2], Daniel C. Koboldt[1], Heather Schmidt[1], Joelle Kalicki[1], Qunyuan Zhang[2,5], Lei Chen[1], Ling Lin[1], Michael C. Wendl[1,2], Joshua F. McMichael[1], Vincent J. Magrini[1,2], Lisa Cook[1], Sean D. McGrath[1], Tammi L. Vickery[1], Elizabeth Appelbaum[1], Katherine DeSchryver[3], Sherri Davies[3], Therese Guintoli[3], Li Lin[3], Robert Crowder[3], Yu Tao[6], Jacqueline E. Snider[3], Scott M. Smith[1], Adam F. Dukes[1], Gabriel E. Sanderson[1], Craig S. Pohl[1], Kim D. Delehaunty[1], Catrina C. Fronick[1], Kimberley A. Pape[1], Jerry S. Reed[1], Jody S. Robinson[1], Jennifer S. Hodges[1], William Schierding[1], Nathan D. Dees[1], Dong Shen[1], Devin P. Locke[1], Madeline E. Wiechert[1], James M. Eldred[1], Josh B. Peck[1], Benjamin J. Oberkfell[1], Justin T. Lolofie[1], Feiyu Du[1], Amy E. Hawkins[1], Michelle D. O'Laughlin[1], Kelly E. Bernard[1], Mark Cunningham[1], Glendoria Elliott[1], Mark D. Mason[1], Dominic M. Thompson Jr[7], Jennifer L. Ivanovich[7], Paul J. Goodfellow[7], Charles M. Perou[8], George M. Weinstock[1,2], Rebecca Aft[7], Mark Watson[9], Timothy J. Ley[1,2,3,4], Richard K. Wilson[1,2,4] & Elaine R. Mardis[1,2,4]

Massively parallel DNA sequencing technologies provide an unprecedented ability to screen entire genomes for genetic changes associated with tumour progression. Here we describe the genomic analyses of four DNA samples from an African-American patient with basal-like breast cancer: peripheral blood, the primary tumour, a brain metastasis and a xenograft derived from the primary tumour. The metastasis contained two *de novo* mutations and a large deletion not present in the primary tumour, and was significantly enriched for 20 shared mutations. The xenograft retained all primary tumour mutations and displayed a mutation enrichment pattern that resembled the metastasis. Two overlapping large deletions, encompassing *CTNNA1*, were present in all three tumour samples. The differential mutation frequencies and structural variation patterns in metastasis and xenograft compared with the primary tumour indicate that secondary tumours may arise from a minority of cells within the primary tumour.

Basal-like breast cancer is characterized by the absence of oestrogen receptor (ER) expression, the lack of *ERBB2* gene amplification, and a high mitotic index. The consequent absence of approved targeted therapy options and frequently poor response to standard chemotherapy often result in a rapidly fatal clinical course. The disease also accounts for an elevated percentage of breast cancers in patients with African ancestry[1]. Clinical progress has been limited by a poor understanding of the genetic events responsible for this tumour subtype and by limited preclinical models to study the disease. Because basal-like breast cancer has a highly unstable genome, a key question is whether the fatal metastatic process is driven by mutations that occur after the tumour cells arrive at the distant site, or whether the primary tumour generates cells with a complete repertoire of somatic mutations required for metastatic growth. The rapid advancement of next-generation sequencing technologies allows comprehensive characterization of genomic changes, facilitating the comparison of multiple samples taken from the same patient to address the genetic basis for tumour progression and metastasis.

Case presentation and previous characterization of samples
A 44-year-old African-American woman was diagnosed with an ERBB2-negative and ER-negative inflammatory breast cancer. She

was treated with neoadjuvant dose-dense chemotherapy[2], but significant residual tumour was present in the breast and axillary lymph nodes at mastectomy. This indicated chemotherapy resistance and she subsequently underwent radiation therapy. Eight months later she developed a cerebellar metastasis and, despite resection, rapidly succumbed to widely disseminated disease. A transplantable human-in-mouse (HIM) xenograft tumour line was generated from a sample of her primary tumour biopsied before treatment[3]. The xenograft in the mammary fat pad was locally invasive and produced metastatic deposits in lymph nodes and ovaries. Informed consent for full genome sequencing was obtained and DNA samples were prepared from her peripheral blood, primary tumour, brain metastasis and an early passage xenograft (harvested 101 days after initial engrafting into the mouse host). Application of the PAM50 intrinsic subtype algorithm identified the primary tumour, brain metastasis and xenograft line as basal-like subtype, with high risk of relapse (ROR) scores[4].

Sequence coverage and mutation analysis
Using a paired-end sequencing strategy, we generated 130.7, 124.9, 111.8 and 149.2 billion base pairs of sequence data from genomic DNA derived from blood, primary tumour, brain metastasis and

xenograft samples, respectively, with corresponding haploid coverages of 38.8×, 29.0×, 32.0× and 23.8× (Supplementary Table 1). These genome-wide coverages were assessed by comparing single nucleotide variants (SNVs) detected by MAQ[5] with single nucleotide polymorphisms (SNPs) genotyped using Illumina 1M duo arrays for all tissues excluding the xenograft. Array data from the metastasis were used as a surrogate for monitoring the xenograft SNP coverage and confirmed bi-allelic detection of 98.27%, 96.79%, 96.17% and 88.77% of the heterozygous array SNPs in the normal, primary tumour, metastasis and xenograft sequence data sets, respectively (Supplementary Table 1).

The process for selecting somatic mutations is shown in Supplementary Table 2 and is detailed in Supplementary Information. Putative somatic SNVs and indels that overlap with coding sequences, splice sites and RNA genes were included as 'tier 1'. We combined tier 1 sites identified in all three tumour samples and obtained deep read count data for all four samples from Illumina and/or 454 platforms (Supplementary Information). On the basis of pathology review, the tumour cellularity estimates were 70% for the primary tumour and 90% for both the brain metastasis and xenograft. Using these estimates, we calculated the tumour read counts by proportionally removing the counts derived from the normal tissue reads from the counts obtained from primary tumour and metastasis reads (Supplementary Table 3a). Using the Illumina platform, we also generated 15.6 Gb (4.4× haploid coverage) of sequence data for the NOD/SCID mouse genome used as the host for the xenograft line. The mapping rates of NOD/SCID data to human and mouse C57BL/6 reference sequences were 3.17% and 95.85%, respectively. As the non-malignant contamination in xenograft is largely from murine cells (which do not significantly affect read mapping), no correction was applied for the xenograft data. Adjusted tumour read counts were used to calculate mutant allele frequencies. Somatic changes were validated by comparing mutant allele frequencies in the three tumour genomes against the germline DNA sample, combined with a manual review of ABI 3730 data from PCR products (Supplementary Information).

A total of 50 somatic sites, including 28 missense, 11 silent, 2 splice site, 1 RNA, 1 nonsense, 4 insertions and 3 deletions, were validated in at least one of the three tumour genomes. Of coding point mutations, the observed nonsynonymous/synonymous ratio of 2.64:1 (29:11) is not significantly different from that expected by chance[6] ($P = 0.51$), indicating that the majority of coding mutations do not confer a selective advantage to the basal tumour. This is similar to the nonsynonymous/synonymous ratio reported in the small-cell lung cancer cell line NCI-H209[7], but higher than the ratio reported in the melanoma cell line COLO-829[8].

Mutation spectrum in basal breast tumour

We investigated the spectrum of DNA sequence changes in this basal tumour and found that 55% (22 out of 40) of coding point mutations represent C•G→T•A transitions. A similar frequency of C•G→T•A

transitions (56% (18 out of 32)) was observed in a lobular breast tumour recently reported[9] (Fig. 1a). In addition, 15% (6 out of 40) of coding point mutations representing C•G→A•T transversions were detected in the basal tumour, but none was found in the lobular tumour. The statistical significance of these observations should be explored with the comparative analysis of a larger number of basal and lobular breast tumours. Moreover, the observed C•G→T•A transition frequency is notably higher than those observed in a previous breast cancer study[10] ($P = 0.027$; Fig. 1b). A set of extremely high-confidence tier 1–4 mutations (somatic score >55 and average mapping quality >79) was used to explore the genome-wide mutation spectrum. We found that mutations at A•T bases are significantly expanded in the genome-wide set compared to the coding mutations, especially for A•T→G•C transitions ($P = 0.0065$). This is consistent with the higher A•T content in non-coding sequences than in coding sequences. Comparison to the whole-genome mutation spectrum reported for the melanoma cell line (COLO-829)[8] and a small-cell lung cancer cell line (NCI-H209)[7] indicates that the tumour genome under study shows no sign of tobacco or ultraviolet influence. We then compared the fraction of the three classes of guanine mutations occurring at CpG dinucleotides in primary tumour, brain metastasis and xenograft and found that the frequencies of G→A mutations are 27.54%, 27.60% and 28.05% in each respective tumour, significantly higher than both the genome average of 4.45% ($P < 10^{-10}$) and the frequency reported in NCI-H209 ($P < 10^{-10}$; Fig. 1c).

Distribution of mutations among tumours

Common mutations detected in three tumour genomes. Of the 50 validated point mutations and small indels, 48 are detectable in all three tumours. We performed a statistical enrichment test that takes the variations of different platforms, experiments and primer pairs into consideration (Supplementary Information). These 48 sites consist of 20 sites with relatively comparable frequencies across tumours, 26 sites significantly enriched (false discovery rate (FDR) ≤ 0.05) in the metastasis and/or xenograft, and two sites with significant enrichment (FDR ≤ 0.05) in the primary tumour (Fig. 2 and Table 1). The affected genes and the likely consequences of these mutations are summarized in Table 1 and Supplementary Table 3b.

Mutations with comparable frequencies in three tumours. We detected a JAK2 mutation (I166T), residing in the FERM domain, which is different from the previously reported activating mutations in myeloproliferative diseases, often found in the pseudokinase domain[11]. Screening of an additional 116 breast tumours identified another mutation (R1122P) in the kinase domain of JAK2 from a luminal B-type breast cancer. A splice site mutation (e8-1) was found in IRAK2. We performed a polymerase chain reaction with reverse transcription (RT–PCR) experiment using RNAs from the brain metastasis and xenograft and found that the first 30 nucleotides of exon 8 (IRAK2, NM_001570) were skipped and an internal exonic AG site was used as a splice acceptor, resulting in an in-frame deletion. A missense
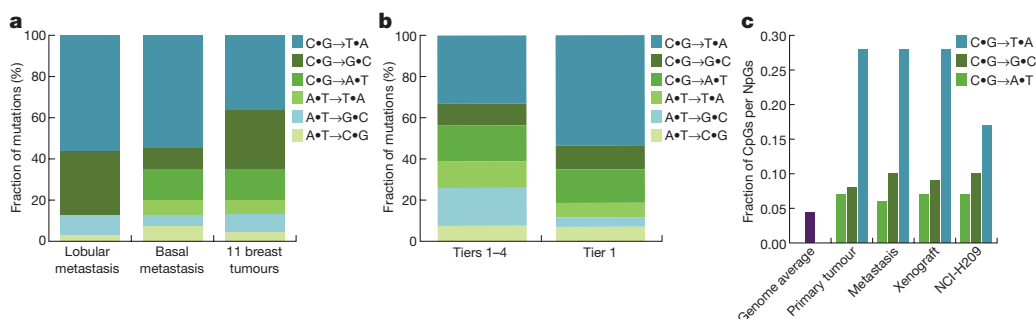

Figure 1 | Mutational signatures in the basal breast tumour. a, Fraction of mutations in each of the transition and transversion categories in the metastasis of a lobular breast tumour[9], the metastasis of the basal breast tumour under study, and the 11 breast tumours reported previously[29] from which 1,104 coding mutations identified in the discovery set were used in the analysis. **b,** Fraction of mutations in each of the transition and transversion categories in 43 tier 1 mutations and 3,204 tier 1–4 mutations in the metastasis under study. **c,** Fraction of guanine mutations at CpGs in primary tumour, metastasis, xenograft and NCI-H209 as reported previously[7].
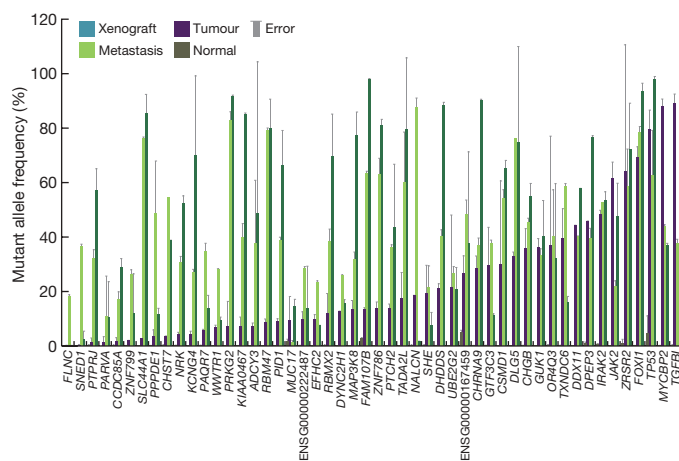
Figure 2 | Mutant allele frequency from deep read count data. The mutant allele frequency of each somatic mutation is shown. Mutations were validated using both 454 and Illumina sequencing. Each bar represents the average of the frequency yielded by the two technologies for a single primer pair and the error bars represent the standard deviation. Data were considered only if there were at least 200 reads from Illumina sequencing and at least 20 reads from 454 sequencing. If no error bar exists, then data were only available from a single sequencing platform.

mutation (A401S) in *CSMD1* was found in all three tumours. Loss of *CSMD1* expression is associated with poor survival in invasive ductal breast carcinoma[12] and it is frequently deleted in colorectal adenocarcinoma and head/neck carcinomas[13]. We also identified three missense (E608K, T1456R, and Q2204R) and one nonsense (Q3005*) mutations in *CSMD1* in four breast cancers out of 116 screened. A binomial test shows that *CSMD1* is significantly mutated in breast cancer ($P = 0.022$ and FDR = 0.197; Supplementary Table 4).

Mutations highly enriched in metastasis and/or xenograft. A missense mutation (A681E) in *NRK*, a protein kinase involved in activating JNK, was found to be present in all three tumours, but at 8- and 13-fold increased allele frequencies in the metastasis and xenograft, respectively (Fig. 2 and Table 1). Two somatic mutations (S424C and Q521*) in *NRK* have been previously reported in breast cancer[14]. The missense mutation (P461L) identified in the carboxy terminus of MAP3K8 was present at a roughly sixfold increase in the xenograft compared to the primary tumour. C-terminal truncation of MAP3K8 has been shown to activate this oncogenic kinase[15,16], raising the possibility that this C-terminal substitution (P461L) is an activating mutation.

Another missense mutation (K1017N) in *PTPRJ*, a protein tyrosine phosphatase, had a mutant allele frequency of 32% in the metastasis and 57% in the xenograft compared with just 1.3% in the primary tumour. This K1017N mutation in *PTPRJ* is among the most highly enriched mutations in both the metastasis (FDR = 0.00035) and xenograft (FDR = 0.00022). The mutation site is in the juxtamembrane domain (a basic residue motif) and is in close proximity to the tyrosine-protein phosphatase domain (amino acids 1041–1298). Reference 17 reported that the PTPRJ charged peptide (amino acids 1013–1024) is responsible for interaction with its substrates, such as ERK1/2. The K1017N mutation found in the basal tumour and the K1016A mutation described in ref. 17 both change a basic residue to a neutral residue, indicating that these two mutations may be functionally similar. A missense mutation (F299V) in *WWTR1*, assigned as deleterious by SIFT[18], was detected at 28% mutant allele frequency in metastasis, but only at 7% and 10% in primary tumour and xenograft, respectively (Fig. 2 and Table 1). WWTR1, a 14-3-3 binding protein with a PDZ binding motif, has been shown to modulate mesenchymal stem cell differentiation[19]. Overexpression of *WWTR1* has also been implicated in promoting the migration, invasion and tumorigenesis of breast cancer cells[20].

Another point mutation (R258Q) was identified in *CHGB* (chromogranin B) encoding a tyrosine-sulphated secretory protein. A SNP at the same position was reported to dbSNP in January 2009 for a Yoruba sample. It was also assigned as a germline site in another African-American with breast cancer when we genotyped this mutation in 112 additional primary tumours and 73 metastatic tumours of various expression classes (Supplementary Information). To investigate this variant further, 84 cancer-free African-American women with an average age of 71.2 years (low risk for developing breast cancer) and 38 early-onset African-American breast cancer patients with an average age of 35.6 years were genotyped. The results indicated that 8 out of 84 controls and 3 out of 38 cases carried the variant allele, indicating that this variant is unlikely to be a breast cancer susceptibility allele.

Three validated indels were enriched in the metastasis and/or xenograft. One was the 1-bp insertion in exon 4 of the *TP53* gene, which creates a frameshift mutation (Q167fs) in the DNA binding domain and results in a truncated protein. We found the *TP53* mutation to be significantly enriched in the xenograft, whereas it was present at a relatively constant frequency in primary tumour and metastasis (Fig. 2 and Table 1).

Mutations enriched in the primary tumour. A nonsense mutation (Q2222*) in *MYCBP2* and a missense mutation (E576K) in *TGFBI*, both found in all three tumours, had higher mutant allele frequencies in the primary tumour (88% for *MYCBP2* and 89% for *TGFBI*) than in the metastasis (44% for *MYCBP2* and 38% for *TGFBI*) or the xenograft (37% for *MYCBP2* and 18% for *TGFBI*) (Fig. 2 and Table 1).

***De novo* mutations identified in the metastasis.** Two *de novo* mutations were discovered in the metastatic tumour, neither of which was detected in the primary or xenograft tumour genomes. One was a missense mutation (T708I) in *SNED1*, with a mutant allele frequency of 37%; the other was a silent mutation (N2483) in *FLNC* with a mutant allele frequency of 18% (Fig. 2 and Table 1). Because the xenograft line, without these two mutations, exhibits metastatic lesions in ovarian, lymphoid and subcutaneous tissue (data not shown), it is unlikely that these mutated genes are essential to the metastatic process.

Elevated copy number alterations in metastasis and xenograft

The cnvHMM algorithm (K.C., X.S., E.R.M., L.D. and R.K.W., unpublished) applied to the aligned sequence reads to detect regions of copy number alterations in all three tumours. Using pathology-based purity estimates for the primary tumour and brain metastasis, we calculated the read depth contributed from the tumour cells alone and then computed the copy number for all genomic positions. Read depth correction was not applied to the xenograft, as stated earlier. We subsequently compared the copy number data from all three tumours with those from peripheral blood, to identify genomic segments with significant copy number alterations (CNAs) (Supplementary Information). A total of 516.5 Mb, 640.4 Mb and 754.5 Mb were amplified, whereas 342.5 Mb, 383.1 Mb and 562.5 Mb were deleted, in primary tumour, metastasis and xenograft, respectively (Supplementary Table 5–7). Moreover, 96.11% and 93.98% of CNA sequences in the primary tumour were also found in CNA segments in the metastasis and xenograft, respectively, indicating that most primary tumour CNAs are preserved during disease progression and engraftment. On the other hand, only 80.65% of metastasis and 61.29% of xenograft CNA sequences overlap with primary tumour CNAs. Furthermore, 155 regions with focal copy number segments (≤2 Mb) were detected in the primary tumour, but only 101 and 97 regions in the metastasis and xenograft (Supplementary Tables 8–10). Our result also shows that 111 (average span = 745,183 bp) and 99 (average span = 799,395 bp) focal copy number segments (≤2Mbp) in the primary tumour overlap with broader copy number segments in the metastasis (average span = 2,245,546 bp) and xenograft (average span = 3,565,456 bp), indicating possible expansion of primary focal

Table 1 | Summary of point mutations and small indels

Chr	Start	Allele change	Gene	Amino acid change	Mutant allele frequency (%)				Copy number			Enrichment FDR	
					N	T	M	X	T	M	X	M:T	X:T
1	26062702	G>A	PAQR7	p.A72	0.17	5.78	34.55	13.70	2	2	2	9.00×10^{-4}	0.011
1	26646672	G>A	DHDDS	p.R159H	0.14	21.12	40.24	88.29	2	2	2	5.73×10^{-5}	2.46×10^{-5}
1	43684654	G>A	KIAA0467	p.G2119R	0.13	7.00	40.02	84.84	2	2	2	0.001	5.98×10^{-5}
1	45068225	C>G	PTCH2	p.W293S	0.02	13.70	36.03	43.61	2	2	2	0.085	0.381
1	152723308	delGCAACTTTTCATT	SHE	p.LPFKG476in_frame_delW	0.19	19.28	21.33	7.69	4.61	5.34	6.92	0.820	0.065
1	226395989	C>A	GUK1	p.P11Q	0.01	36.29	33.12	40.17	3.66	3.96	4.64	0.374	0.365
1	242935580	A>T	PPPDE1	p.T151S	0.12	3.39	48.57	11.47	3.45	3.71	4.38	0.012	0.063
2	24994872	G>A	ADCY3	p.H163	0.06	7.10	37.49	48.71	3.17	3.24	3.78	0.007	0.029
2	56273320	delG	CCDC85A	p.E161fs	0.16	1.71	17.11	28.78	2.9	3.24	3.34	0.002	0.006
2	197349569	G>C	GTF3C3	p.R474G	0.11	29.42	37.75	11.08	1.4	1.31	1.24	0.316	0.065
2	229835724	C>T	PID1	p.S14	0.11	8.95	38.89	66.13	2	2	1.36	0.001	0.166
2	241641282	C>T	SNED1	p.T708I	0.04	0.32	36.52	2.30	2	2	2	1.58×10^{-4}	0.719
3	10236363	G>T	IRAK2	e8-1	0.38	48.37	52.69	53.33	2	2	2	0.156	0.762
3	139505123	G>A	TXNDC6	p.R221W	0.29	39.50	58.62	15.81	2	2	2	0.039	0.012
3	150728323	A>C	WWTR1	p.F299V	0.03	6.87	28.14	9.53	2	2	2	1.43×10^{-4}	0.020
4	40051165	C>A	CHRNA9	p.D437E	0.10	28.38	36.82	90.26	2	2	2	0.073	9.67×10^{-5}
4	40134827	delG	RBM47	p.I280fs	0.05	8.62	79.15	79.74	2	2	2	0.030	0.124
4	82232630	C>T	PRKG2	p.R709	0.11	6.99	82.99	91.51	2	2	2	0.083	0.094
5	135422725	G>A	TGFBI	p.E576K	0.17	89.09	37.58	18.45	2	2	2	3.34×10^{-6}	3.23×10^{-5}
5	169466048	C>T	FOXI1	p.S170F	0.15	69.28	78.33	93.61	2	2	2	0.473	0.009
7	100463999	G>C	MUC17	p.S861T	1.69	9.22	1.46	14.43	2	2.76	4.04	0.073	0.816
7	128284099	C>T	FLNC	p.N2483	0.11	0.17	18.21	0.16	2.54	2.8	2.93	0.002	0.193
7	148400407	G>A	ZNF786	p.F130	0.13	13.61	62.86	81.04	2.51	2.85	3.54	3.01×10^{-4}	3.23×10^{-5}
8	3232441	C>A	CSMD1	p.A409S	0.04	29.75	54.22	65.18	2	2	2	0.355	0.141
8	8477326	C>T	ENSG00000222487	NULL	0.11	9.61	28.43	13.74	2	2	2.67	0.120	0.787
9	5040714	T>C	JAK2	p.I166T	0.09	61.63	21.93	47.40	2.83	2.67	2.84	0.246	0.999
9	107137789	G>A	SLC44A1	p.A132T	0.08	2.59	76.14	85.31	2	1.29	1.19	1.43×10^{-4}	1.05×10^{-4}
10	14603968	C>T	FAM107B	p.R237Q	2.65	13.53	63.25	97.88	3.7	4.04	4.76	3.29×10^{-6}	8.54×10^{-8}
10	30789749	C>T	MAP3K8	p.P461L	0.11	13.33	31.72	77.47	3.44	3.71	4.21	0.002	9.67×10^{-5}
10	79240899	G>A	DLG5	p.D1474	0.07	32.94	76.10	74.72	2	2	2	6.12×10^{-5}	0.011
11	12496610	insATGGAG	PARVA	p.338in_frame_insDG	0.00	1.41	10.75	10.58	2	2	2	0.347	0.365
11	48128224	A>T	PTPRJ	p.K1017N	0.20	1.25	32.08	57.23	2	2	2.99	3.48×10^{-4}	2.20×10^{-4}
11	102687902	G>A	DYNC2H1	p.R3867Q	0.06	12.81	25.78	15.69	2	2	2	0.002	0.023
12	31122692	T>G	DDX11	p.V33G	0.02	44.35	40.39	57.88	1.49	1.37	1.24	0.316	0.386
13	76628331	G>A	MYCBP2	p.Q2222*	0.10	87.84	43.76	36.95	2	2	2	0.004	0.003
13	100688137	A>T	NALCN	p.D468E	0.16	18.60	87.66	1.65	2	2.74	2.92	0.004	0.216
14	19285546	G>T	OR4Q3	p.L40	0.22	36.94	40.31	32.28	2	2	2	0.313	0.107
16	66569387	T>G	DPEP3	p.R262S	0.84	45.61	39.43	76.59	2	2.9	3.02	0.293	6.93×10^{-4}
16	82828230	C>A	KCNG4	p.G121	0.04	4.15	26.82	69.89	2.43	3.09	3.49	0.083	0.259
17	7519157	insG	TP53	p.Q167fs	4.61	79.40	62.62	97.96	2	2	2	0.085	0.003
17	32904736	C>T	TADA2L	p.R339W	0.12	17.49	59.92	79.47	2	2	2	0.002	0.002
19	12363315	G>A	ZNF799	p.H299	0.17	2.05	26.23	11.81	2	2	3.06	0.062	0.618
19	16006577	insA	ENSG00000167459	p.I38fs	4.82	26.53	48.47	37.74	2	2	3.06	0.286	0.809
20	5851563	G>A	CHGB	p.R258Q	0.14	35.64	45.50	54.87	2.57	2.86	3.64	0.057	0.005
21	45015744	G>A	UBE2G2	p.I158	0.12	21.57	26.72	20.89	2	2	2	0.522	0.728
X	15731812	C>G	ZRSR2	p.A95G	1.01	64.01	58.66	72.08	2.51	2.77	2.99	0.137	0.969
X	43893087	C>G	EFHC2	e15-1	0.01	9.88	23.15	7.35	2	2.68	2.82	0.114	0.381
X	46318872	insA	CHST7	p.T188fs	0.19	3.67	54.36	38.84	2	2.68	2.82	0.073	0.058
X	105040331	C>A	NRK	p.A681E	0.12	4.08	30.84	52.45	2	2	2	0.085	0.017
X	129374039	A>G	RBMX2	p.K169E	0.30	11.88	38.36	69.46	2	2.65	2.77	0.002	0.003

Gene sets from Ensembl build 54 and GenBank (downloaded in May 2009) were used for annotation of mutations. Enrichment FDR represents the false discovery rate of the significance of the variant frequency change between the two samples. M, metastasis; N, peripheral blood; T, primary tumour; X, xenograft.
* Nonsense mutation.

regions or selection of new adjacent events during disease progression and in the mouse host. Sequence depth-based copy number analysis shows overall the highest concordance with other platforms, including the array CGH and Illumina SNP array, and also provided the highest concordance of copy number (correlation coefficients: 0.89–0.97) between primary tumour, metastasis and xenograft (Supplementary Table 11).

Common and unique structural variations in three tumours

We used BreakDancer[21] to detect structural variants in sequencing data from paired end libraries (Supplementary Table 12) and applied a set of thresholds to identify putative somatic structural events.
Deletions, insertions and inversions. Breakpoint-containing contigs from the three tumour samples that were not present in the matched normal genome were successfully assembled for 137 deletions, 15 insertions and 38 inversions using the TIGRA assembler (L.C., K.C., J.W.W., E.R.M., R.K.W., L.D. and G.M.W., unpublished), suggesting that they were putative somatic events. We then re-mapped individual reads to these assembled contigs to screen

out germline structural variants and to confirm somatic structural variants (Supplementary Information), resulting in the detection of 59 deletions and 18 inversions. PCR primers were designed successfully to validate 73 out of 77 putative structural variant events and the resulting amplicons were sequenced by either the Roche 454 or ABI 3730 platform. Subsequently, 28 deletions and 6 inversions were validated as somatic events (Table 2). Among them, a 46,462-bp heterozygous deletion in FBXW7 removes the last 10 exons and a portion of the first exon of NM_018315, probably inactivating FBXW7. FBXW7 targets cyclin E and mTOR for ubiquitin-mediated degradation[22,23]. Numerous cancer-associated mutations in FBXW7 have been previously reported, and loss of FBXW7 function causes chromosomal instability and tumorigenesis[24]. Two overlapping deletions (538,467 bp and 515,465 bp in length) on chromosome 5, affecting CTNNA1 along with LRRTM2, MATR3, SNORA74A and SIL1, were also validated. This result is consistent with the detection of a focal copy number deletion encompassing this region in both metastasis (copy number = 0.65) and xenograft (copy number = 0.03) (Fig. 3 and Supplementary Tables 9 and 10). Careful examination of

Table 2 | Validated structural variations

Type	Tumour source	Chromosome A	Breakpoint A	Orientation A	Chromosome B	Breakpoint B	Orientation B	Event size (bp)	Gene
Translocation	T,M,X	1	245548334	Minus	2	64855174	Plus	–	*ZNF496*
Translocation	T,M	1	245548342	Plus	6	144243130	Plus	–	*ZNF496, C6orf94*
Translocation	T,M,X	2	64855565	Plus	6	144243118	Minus	–	*C6orf94*
Translocation	T,M,X	2	165126335	Plus	16	4537866	Plus	–	*GRB14*
Translocation	T,M,X	4	188855443	Plus	9	139022260	Plus	–	*ABCA2*
Translocation	T,M,X	12	10874022	Plus	14	99382256	Minus	–	*EML1*
Translocation	T,M	19	17188977	Minus	3	188010735	Plus	–	*USE1*
Inversion	T,M,X	1	35703682	–	1	35732148	–	28,465	*KIAA0319L*
Inversion	T,M,X	1	95919529	–	1	95920940	–	1,410	–
Inversion	T,M,X	1	204459097	–	1	204461297	–	2,200	–
Inversion	T,M,X	1	204459547	–	1	204460581	–	1,033	–
Inversion	T,M,X	4	177886041	–	4	177890171	–	4,129	*VEGFC*
Inversion	T,M,X	19	17800861	–	19	17801858	–	996	*JAK3*
Deletion	M	1	29389213	–	1	29416133	–	26,919	*MECR*
Deletion	T,M,X	1	76496719	–	1	76496797	–	79	*ST6GALNAC3*
Deletion	T,M,X	1	88291885	–	1	88292292	–	406	–
Deletion	T,M,X	2	18629189	–	2	19196656	–	567,466	*NT5C1B*
Deletion	T,M,X	2	64853205	–	2	65010694	–	157,488	–
Deletion	T,M,X	2	128745303	–	2	128898612	–	153,308	*HS6ST1*
Deletion	T,M,X	4	1203395	–	4	1265560	–	62,164	*CTBP1*
Deletion	T,M,X	4	135737399	–	4	135738718	–	1,318	–
Deletion	T,M,X	4	147221480	–	4	147294628	–	73,147	*AK057233*
Deletion	T,M,X	4	153446894	–	4	153493357	–	46,462	*FBXW7*
Deletion	T,M,X	5	15572469	–	5	15572649	–	179	*FBXL7*
Deletion	T,M,X	5	130743604	–	5	130743718	–	113	*CDC42SE2*
Deletion	T,M,X	5	138131495	–	5	138669963	–	538,467	*CTNNA1, LRRTM2, MATR3, SNORA74A, SIL1*
Deletion	T,M,X	5	138141753	–	5	138657219	–	515,465	*CTNNA1, LRRTM2, MATR3, SNORA74A, SIL1*
Deletion	T,M,X	6	39689264	–	6	39689652	–	387	*KIF6*
Deletion	T,M,X	7	999743	–	7	999984	–	240	–
Deletion	T,M,X	7	135419232	–	7	135419453	–	220	–
Deletion	T,M,X	8	32597100	–	8	32706664	–	109,563	*NRG1*
Deletion	T,M,X	8	116552846	–	8	116634665	–	81,818	*TRPS1*
Deletion	T,M,X	8	136595795	–	8	136596285	–	489	*KHDRBS3*
Deletion	T,M,X	9	2746534	–	9	2746735	–	200	–
Deletion	T,M,X	10	77142378	–	10	77142881	–	502	*C10orf11*
Deletion	T,M,X	11	115974418	–	11	115974688	–	269	–
Deletion	T,M,X	11	125479377	–	11	125479744	–	366	–
Deletion	T,M,X	17	24451601	–	17	24475255	–	23,653	*MYO18A*
Deletion	T,M,X	17	73733446	–	17	73733547	–	100	*BIRC5*
Deletion	T,M,X	18	46765510	–	18	46768017	–	2,507	*ELAC1*
Deletion	T,M,X	X	149511547	–	X	149548642	–	37,094	*MTM1*

M, metastasis; T, primary tumour; X, xenograft.

this region in the aligned sequence reads for the primary tumour confirms the existence of copy number deletion. Loss of *CTNNA1* was shown to result in global loss of cell adhesion in human breast cancer cells[25] and increased *in vitro* tumorigenic characteristics[26], indicating that this bi-allelic deletion has functional importance. A 109,563-bp heterozygous deletion on chromosome 8 was assembled and validated in all three tumours. This event removed three exons of *NRG1*, which encodes a peptide growth factor that binds to ERBB3 and ERBB4. Notably, a 26,919-bp deletion in *MECR* was only identified, assembled and validated in the metastasis, suggesting its *de novo* nature in this sample.

Translocations. Of the 112 assembled putative translocations, 34 passed manual review using Pairoscope graphs (D.E.L., C.C.H., E.R.M., L.D. and R.K.W., unpublished), and 19 with an assembly score greater than our experimentally supported cutoff of 10 were included in Supplementary Table 13. Seven translocations were experimentally validated (Table 2). One validated translocation t(4;9)(188855443;139022258), assembled in all three tumours, involved a long terminal repeat (LTR) from the ERVL-MaLR family on chromosome 4 and *ABCA2* on chromosome 9. The translocation removes the final exon of the *ABCA2* gene (NM_001606). Two other validated translocations, identified in all three tumours, are t(1;2)(245548338;64855172) and t(2;6)(64855607;144243116) (Supplementary Fig. 1). Noticeably, the breakpoints on chromosome 2 for these two translocations are only separated by 393 bp in a TcMar-Tigger repeat. The chromosome 1 breakpoint of t(1;2)(245548338;64855172) is in intron 5 of NM_032752 in *ZNF496*. We expect the translation of *ZNF496* to continue through exon 5 into intron 5 due to lack of a splice acceptor site. On the other hand, t(2;6)(64855565;144243116)

involves *FAM164B* on chromosome 6 and the translocation contig retains three exons of XM_928657. We have also validated t(1;6)(245548342;144243110) (not detected by BreakDancer), the breakpoints of which are only 4 bp and 6 bp away from the breakpoints identified on chromosomes 1 and 6 for t(1;2)(245548338;64855172) and t(2;6)(64855607;144243116), respectively (Supplementary Fig. 1). This translocation is found in both the primary tumour and the metastasis, but apparently is lost in the xenograft (Supplementary Fig. 1 and Fig. 4). Sequencing of two PCR products generated using two primer pairs from chromosomes 1 and 6 demonstrated the presence of two forms of genomic fusion: one includes chromosomes 1 and 6 and the other includes chromosomes 1, 2 and 6. The former is only present in the primary tumour and the metastasis.

Discussion

Our comprehensive analysis of this sample set identified 50 novel somatic point mutations and small indels in coding sequences, RNA genes and splice sites as well as 28 large deletions, 6 inversions and 7 translocations. In terms of functional annotation, a hierarchy can be suggested. The first level includes somatic changes likely to be functional, such as the small indel in *TP53*, the large heterozygous deletion in *FBXW7* and the bi-allelic deletion in *CTNNA1*. The second level consists of nonsynonymous mutations in genes previously noted to be targeted for somatic mutation in cancer or found to be recurrently mutated in this study, although the exact mutations are novel and their functional importance requires further investigation (*JAK2*, *PTCH2*, *CSMD1* and *NRK*). The third level contains mutations known to be related to signal transduction in the malignant cells and/or found to be enriched during disease progression (*MAP3K8*,
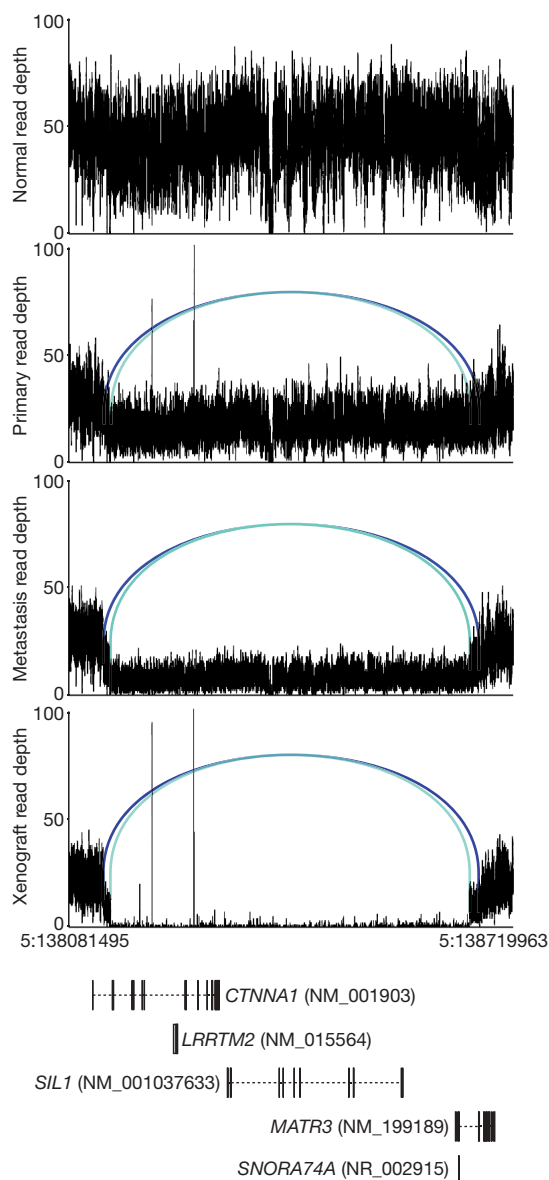
Figure 3 | Two overlapping *CTNNA1* deletions on chromosome 5 in three tumours. A graph of sequence depths, read pairs and genes in a 638,468-bp region containing two overlapping deletions. The top four panels display the read depths at each base, and the reads within the region whose mates mapped at an abnormal distance are displayed as blue bars, with matched pairs connected by arcs. Two different shades of blue indicate the two separate allelic deletion events (538,467 bp and 515,465 bp in length). The bottom panel displays genes annotated in this genomic region.

PTPRJ and *WWTR1*). The final level, by far the largest group, awaits the acquisition of new data. Analysis of germline variants for over 500 classic tumour suppressor genes and oncogenes[27] identified a large number of SNPs, none of which was an unequivocal hereditary breast cancer susceptibility allele (data not shown).

The wide range of mutant allele frequencies suggests considerable genetic heterogeneity in the cellular population at the primary site. The mutation frequency range narrowed in brain metastasis and xenograft, indicating that the metastatic and transplantation processes selected for cells carrying a distinct subset of the primary tumour mutation repertoire. The overlap between the mutation frequency changes seen in the metastatic and xenograft samples argues that cellular selection during xenograft formation is similar to that during metastasis. Moreover, it suggests that the changes were not therapy-related, as the xenograft was established before any treatment. GO annotation of enriched mutations suggests that transcription factor activity is
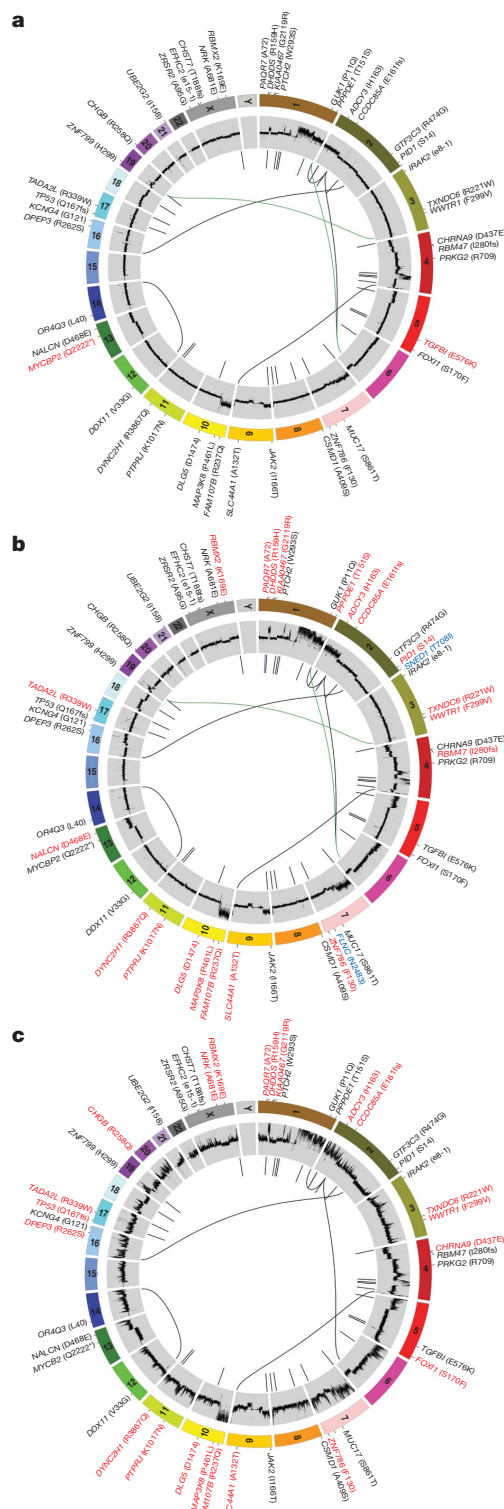
Figure 4 | Circos plots for the primary tumour, metastasis and xenograft genomes. a–c, Circos[30] plots display the validated tier 1 somatic mutations, DNA copy number and validated structural rearrangements in the primary tumour (**a**), metastasis (**b**) and xenograft (**c**). Mutations enriched in the primary tumour are labelled in red in panel **a**; mutations enriched in the metastasis or xenograft are in red in panels **b** and **c**. Mutations and the large deletion unique to the metastasis are in blue (**b**). Translocations only present in primary tumour and metastasis are in green. All shared events are in black. The copy number difference between the tumour and normal is shown (scale: −4 to 4). No purity-based copy number corrections were used for plotting.

possibly selected for in the xenograft (Supplementary Table 14). In contrast to our observation of only two new tier 1 mutations at the metastatic site, sequencing of an indolent metastatic lobular breast tumour showed that the great majority of the mutations detected were completely novel when compared to the primary tumour[9]. However, in this instance, the metastatic process evolved over 9 years, as opposed to less than 1 year in the case we describe here. Another difference relative to the lobular cancer genome, where no structural variants were validated, was that paired-end sequencing detected 41 structural variations within this basal-like tumour genome. Our study of a primary tumour–metastasis–xenograft trio therefore demonstrates that, although additional somatic mutations, copy number alterations and structural variations do occur during the clinical course of the disease, most of the original mutations and structural variants present in the primary tumour are propagated. The preservation of all primary mutations in the xenograft suggests that early passage xenograft lines are valid for functional and therapeutic studies. However, the altered mutation frequency and elevated degree of copy number alterations suggest caution when interpreting the results of such experiments.

The first completed basal-like breast cancer genome is highly complex, as would be anticipated for a tumour type associated with chromosomal instability and DNA repair defects. Indeed, this cancer genome, in comparison with the two AML (acute myeloid leukemia) cases published recently[27,28], revealed a 3–4-fold increase in high-confidence SNVs genome-wide, suggesting a much greater background mutation rate. Future studies should extend our analysis approach of primary, metastatic and normal tissue trios and include affected individuals with diverse geographic origins to produce a complete catalogue of recurrent somatic and inherited variants associated with the development of this common malignancy.

METHODS SUMMARY

Illumina reads from peripheral blood, primary tumour, metastasis and xenograft were aligned to NCBI build36 using MAQ[5] and coverage levels were defined by comparison of SNPs identified by Illumina 1M duo arrays to SNVs called by MAQ. Somatic mutations were identified using our in-house programs glfSomatic and a modified version of the Samtools indel caller (http://samtools.sourceforge.net/). Putative variants were manually reviewed and then validated by Illumina, 3730 or 454 sequencing. Structural variations were identified using BreakDancer[21], manually reviewed and validated by a combination of localized Illumina read assembly, PCR and either 3730 or 454 sequencing. A complete description of the materials and methods used to generate this data set and results is provided in the Supplementary Information.

1. Carey, L. A. et al. Race, breast cancer subtypes, and survival in the Carolina Breast Cancer Study. J. Am. Med. Assoc. 295, 2492–2502 (2006).
2. Citron, M. L. et al. Randomized trial of dose-dense versus conventionally scheduled and sequential versus concurrent combination chemotherapy as postoperative adjuvant treatment of node-positive primary breast cancer: first report of Intergroup Trial C9741/Cancer and Leukemia Group B Trial 9741. J. Clin. Oncol. 21, 1431–1439 (2003).
3. Kuperwasser, C. et al. Reconstruction of functionally normal and malignant human breast tissues in mice. Proc. Natl Acad. Sci. USA 101, 4966–4971 (2004).
4. Parker, J. S. et al. Supervised risk predictor of breast cancer based on intrinsic subtypes. J. Clin. Oncol. 27, 1160–1167 (2009).
5. Li, H., Ruan, J. & Durbin, R. Mapping short DNA sequencing reads and calling variants using mapping quality scores. Genome Res. 18, 1851–1858 (2008).
6. Bardelli, A. et al. Mutational analysis of the tyrosine kinome in colorectal cancers. Science 300, 949 (2003).
7. Pleasance, E. D. et al. A small-cell lung cancer genome with complex signatures of tobacco exposure. Nature 463, 184–190 (2010).
8. Pleasance, E. D. et al. A comprehensive catalogue of somatic mutations from a human cancer genome. Nature 463, 191–196 (2010).
9. Shah, S. P. et al. Mutational evolution in a lobular breast tumour profiled at single nucleotide resolution. Nature 461, 809–813 (2009).
10. Sjoblom, T. et al. The consensus coding sequences of human breast and colorectal cancers. Science 314, 268–274 (2006).
11. Mullighan, C. G. et al. JAK mutations in high-risk childhood acute lymphoblastic leukemia. Proc. Natl Acad. Sci. USA 106, 9414–9418 (2009).
12. Kamal, M. et al. Loss of CSMD1 expression is associated with high tumour grade and poor survival in invasive ductal breast carcinoma. Breast Cancer Res. Treat. doi: 10.1007/s10549-009-0500-4 (2009).
13. Toomes, C. et al. The presence of multiple regions of homozygous deletion at the CSMD1 locus in oral squamous cell carcinoma question the role of CSMD1 in head and neck carcinogenesis. Genes Chromosom. Cancer 37, 132–140 (2003).
14. Stephens, P. et al. A screen of the complete protein kinase gene family identifies diverse patterns of somatic mutations in human breast cancer. Nature Genet. 37, 590–592 (2005).
15. Gandara, M. L., Lopez, P., Hernando, R., Castano, J. G. & Alemany, S. The COOH-terminal domain of wild-type Cot regulates its stability and kinase specific activity. Mol. Cell. Biol. 23, 7377–7390 (2003).
16. Clark, A. M., Reynolds, S. H., Anderson, M. & Wiest, J. S. Mutational activation of the MAP3K8 protooncogene in lung cancer. Genes Chromosom. Cancer 41, 99–108 (2004).
17. Sacco, F. et al. Tumor suppressor density-enhanced phosphatase-1 (DEP-1) inhibits the RAS pathway by direct dephosphorylation of ERK1/2 kinases. J. Biol. Chem. 284, 22048–22058 (2009).
18. Ng, P. C. & Henikoff, S. SIFT: Predicting amino acid changes that affect protein function. Nucleic Acids Res. 31, 3812–3814 (2003).
19. Hong, J. H. et al. TAZ, a transcriptional modulator of mesenchymal stem cell differentiation. Science 309, 1074–1078 (2005).
20. Chan, S. W. et al. A role for TAZ in migration, invasion, and tumorigenesis of breast cancer cells. Cancer Res. 68, 2592–2598 (2008).
21. Chen, K. et al. BreakDancer: an algorithm for high-resolution mapping of genomic structural variation. Nature Methods 6, 677–681 (2009).
22. Zhang, W. & Koepp, D. M. Fbw7 isoform interaction contributes to cyclin E proteolysis. Mol. Cancer Res. 4, 935–943 (2006).
23. Mao, J. H. et al. FBXW7 targets mTOR for degradation and cooperates with PTEN in tumor suppression. Science 321, 1499–1502 (2008).
24. Welcker, M. & Clurman, B. E. FBW7 ubiquitin ligase: a tumour suppressor at the crossroads of cell division, growth and differentiation. Nature Rev. Cancer 8, 83–93 (2008).
25. Bajpai, S., Feng, Y., Krishnamurthy, R., Longmore, G. D. & Wirtz, D. Loss of α-catenin decreases the strength of single E-cadherin bonds between human cancer cells. J. Biol. Chem. 284, 18252–18259 (2009).
26. Plumb, C. L. et al. Modulation of the tumor suppressor protein α-catenin by ischemic microenvironment. Am. J. Pathol. 175, 1662–1674 (2009).
27. Mardis, E. R. et al. Recurring mutations found by sequencing an acute myeloid leukemia genome. N. Engl. J. Med. 361, 1058–1066 (2009).
28. Ley, T. J. et al. DNA sequencing of a cytogenetically normal acute myeloid leukaemia genome. Nature 456, 66–72 (2008).
29. Wood, L. D. et al. The genomic landscapes of human breast and colorectal cancers. Science 318, 1108–1113 (2007).
30. Krzywinski, M. et al. Circos: an information aesthetic for comparative genomics. Genome Res. 19, 1639–1645 (2009).

Author Contributions E.R.M., L.D., R.S.F., M.J.E., T.J.L. and R.K.W. designed the experiments. L.D. and M.J.E. led data analysis. L.D., D.E.L., K.C., J.W.W., C.C.H., M.D.M., D.C.K., Q.Z., H.S., J.K., L.C., L.L., M.C.W., N.D.D., D.S., D.M.T., J.L.I., P.J.G., J.S.H., W.S., G.M.W. and Y.T. performed data analysis. D.E.L., C.C.H., J.W.W., J.F.M. and L.D. prepared figures and tables. R.S.F., L.L.F., R.M.A., J.H., K.D.D., C.C.F., K.A.P., J.S.Re., J.S.Ro., V.J.M., L.C., S.D.M., T.L.V., E.A., K.D., S.D., T.G., L.L., R.C., J.E.S., D.P.L., M.E.W., M.C., G.E., M.D.M., D.M.T., J.L.I. and P.J.G. performed laboratory experiments. S.L. and M.J.E. created the xenograft line. M.J.E., M.W. and R.A. provided samples. D.J.D., S.M.S., A.F.D., G.E.S., C.S.P., J.M.E., J.B.P., B.J.O., J.T.L., F.D., A.E.H., M.D.O. and K.E.B. provided informatics support. L.D., M.J.E., E.R.M. and R.K.W. wrote the manuscript. T.J.L., D.E.L., M.C.W., D.C.K. and C.M.P. critically read and commented on the manuscript.

Author Information The sequence data and high-quality variants have been deposited in the dbGaP database under the accession number phs000245.v1.p1. Reprints and permissions information is available at www.nature.com/reprints. The authors declare no competing financial interests. Correspondence and requests for materials should be addressed to R.K.W. (rwilson@wustl.edu).